Research Square

Preprints are preliminary reports that have not undergone peer review.
They should not be considered conclusive, used to inform clinical practice,
or referenced by the media as validated information.

Effect of continuity plate size on the hysteretic response of a welded moment connection between an HEA beam and a square hollow structural section column

William G. Piraquive
Pontificia Universidad Javeriana
Miguel A. Morales
Pontificia Universidad Javeriana
Fabián A. Lamus
fabian.lamus@escuelaing.edu.co
Escuela Colombiana de Ingenieria Julio Garavito
Federico A. Nuñez
Pontificia Universidad Javeriana

Research Article

Keywords: Beam-to-column connection, Hollow structural section, Continuity plates, Hysteretic behavior, Energy dissipation, Finite element analysis

Posted Date: November 20th, 2026

DOI: https://doi.org/10.21203/rs.3.rs-11683783/v1

License: This work is licensed under a Creative Commons Attribution 4.0 International License.
Read Full License

Additional Declarations: No competing interests reported.

Effect of continuity plate size on the hysteretic response of a welded moment connection between an HEA beam and a square hollow structural section column

William G. Piraquive[1], Miguel A. Morales[1], Fabián A. Lamus[2*], Federico A. Nuñez[1]

[1] Department of Civil Engineering, Faculty of Engineering, Pontificia Universidad Javeriana, Bogotá, Colombia

[2] Faculty of Civil Engineering, Escuela Colombiana de Ingeniería Julio Garavito, Bogotá, Colombia

***Corresponding author:** Fabián A. Lamus, fabian.lamus@escuelaing.edu.co

Author e-mail addresses and ORCID iDs

Willian G. Piraquive: w_gonzalez@javeriana.edu.co; ORCID: 0000-0003-0446-0082

Miguel A. Morales: miguel.morales@javeriana.edu.co;

Fabián A. Lamus: fabian.lamus@escuelaing.edu.co;

Federico A. Nuñez: fnunez@javeriana.edu.co; ORCID: 0000-0002-6011-6553

Abstract

Square hollow structural section (HSS) columns combined with light European HEA beams are an economical option for low-rise steel moment frames, such as those of social housing, but this combination is not covered by the prequalified connections of ANSI/AISC 358 or by the Colombian seismic code NSR-10. This study evaluates a welded moment connection between an HEA100 beam and a 150 × 150 × 9 mm square HSS column in which the beam flanges are joined to the column through two square continuity plates with complete-joint-penetration welds. A three-dimensional nonlinear finite element model was developed in ANSYS and validated against a full-scale cyclic test of a specimen with 190 mm × 12.7 mm plates. After calibrating the flexibility of the test supports, the model reproduced the positive peak force within 3% and the dissipated energy within 7%. A parametric study of 25 configurations, combining five plate side lengths (180–220 mm) and five thicknesses (8–19 mm), was then carried out under the cyclic loading protocol of ANSI/AISC 341 and NSR-10. At a connection rotation of 0.04 rad, the moment at the column face reached 1.64–1.71 times the beam plastic moment in all configurations, well above the minimum of 0.8 required for special moment frames. The maximum moment increased with the plate side length and was practically insensitive to the thickness, the initial stiffness increased with both parameters, and the energy dissipated within ±0.04 rad increased with thickness and decreased with side length, ranging from 4.45 to 5.19 kJ.

Keywords Beam-to-column connection · Hollow structural section · Continuity plates · Hysteretic behavior · Energy dissipation · Finite element analysis

1 Introduction

Post-earthquake reconnaissance has repeatedly shown that severe damage and collapse of steel moment-resisting frames are frequently associated with local failures in beam-to-column connections and in the regions intended to develop plastic hinges. These failures may originate from deficient materials, poor workmanship or design errors, and they limit the capacity of the frame to dissipate energy through stable inelastic deformation of the protected zones. The 1994 Northridge earthquake was a turning point in this respect: the unexpected brittle fractures observed in welded beam-to-column connections of steel moment frames [1] led to the FEMA/SAC program, which produced new design criteria and an experimental qualification framework for moment connections [2].

Since then, moment connections used in special and intermediate steel moment frames in the United States must belong to connection types whose cyclic performance has been demonstrated by testing. The American Institute of Steel Construction (AISC) compiles these connections in ANSI/AISC 358 [3], whereas ANSI/AISC 341 [4] defines the qualification test protocol and its acceptance criteria. Both documents are the basis of the steel provisions in Title F of the Colombian seismic code NSR-10 [5]. Some prequalified connections result from sponsored or patented research and remain proprietary; their use may therefore require the payment of royalties, which increases project costs.

Owing to the large number of possible member combinations, many connections, particularly those between light sections, still lack evidence of their seismic behavior, and designers are restricted to configurations supported by experimental or numerical evidence [6]. This limitation is especially severe in small projects such as social housing, in which light steel sections are sufficient for the gravity loads and the architectural requirements.

Hollow structural sections (HSS) are attractive as columns because of their torsional stiffness, their flexural stiffness about both axes and their high strength-to-weight ratio. Their cyclic flexural behavior has been characterized experimentally and numerically, and the width-to-thickness ratios have been shown to govern local buckling and rotation capacity [6–8]. Connecting open-section beams to HSS columns is, however, complicated by the flexibility of the tube wall, which cannot resist the concentrated forces transferred by the beam flanges without reinforcement. Design guidance for these joints, including internal, through and external diaphragm details, is given in the CIDECT design guides [9, 10].

Several studies have examined the role of diaphragms and external stiffeners in this type of joint. Ting et al. [11] used finite element (FE) analyses to compare box-column to I-beam connections stiffened externally with triangular plates, angles and T-stiffeners, and Shanmugam et al. [12] tested seven full-size externally stiffened connections under cyclic loading, observing failures by weld fracture or by excessive yielding of the stiffeners followed by local buckling. Qin et al. [13] tested full-scale through-diaphragm connections to concrete-filled rectangular tubular columns and showed that modifying the diaphragm geometry considerably improved energy dissipation. Bagheri Sabbagh et al. [14] used FE analyses to develop external diaphragm details for I-beam-to-circular hollow section joints and found that the width of the diaphragm plates controls the distortion of the column wall and the strain concentrations in the diaphragms. In Colombia, Ramírez Ortiz et al. tested [15] and modeled [16] an external diaphragm connection between steel beams and concrete-filled tubular columns; the specimen reached a

beam rotation of 0.07 rad while keeping a moment above 80% of the beam capacity, and the validated model was used to extend the assessment to several European I-shaped beams. These works, together with other validated three-dimensional FE models of beam-to-column joints [17, 18], show that numerical simulation calibrated against tests is a reliable tool to characterize the moment–rotation response of connections and to explore the influence of their geometric parameters.

Other studies have addressed alternative details. López-Colina et al. [19] characterized the main component of welded I-beam-to-RHS-column connections in which beam and column have the same width, so that the flange forces are transferred directly to the side walls of the tube. The Salerno group has studied connections in which the I-beam passes through the hollow column, first for circular [20] and then for square columns with IPE beams, for which a predictive formulation of the rotational ductility was derived from simplified cyclic models [21]. For external diaphragms in square concrete-filled columns, Tjahjanto et al. [22] assessed the axial capacity of the diaphragm plates with FE analyses.

Most of these studies, however, addressed concrete-filled or larger columns, other connection details, or monotonic behavior. To the authors' knowledge, the influence of the size of external diaphragm (continuity) plates on the cyclic response of welded connections between light HEA beams and unfilled square HSS columns has not been quantified. Local qualification studies, such as that of Andrade [23] on I-beams connected to the weak axis of the column, have also shown the need for evidence specific to the sections available in the Colombian market.

This study evaluates a moment connection between an HEA100 beam and a PTE150×150×9 square HSS column (PTE, *perfil tubular estructural*, is the Colombian commercial designation for cold-formed square HSS), in which the beam flanges are joined to the column through two square continuity plates welded around the perimeter of the column, which is not interrupted, so that the plates act as external diaphragms. All joints use complete-joint-penetration (CJP) welds. This combination of sections is not included in ANSI/AISC 358 [3] or in NSR-10 [5] and could be a low-cost alternative for low-rise frame buildings. A nonlinear FE model of the connection was first validated against a full-scale cyclic test and then used to analyze 25 configurations with different continuity plate side lengths and thicknesses. The moment–rotation response, the maximum moment and the dissipated energy of each configuration were evaluated and compared with the acceptance criteria of NSR-10, providing a starting point for the future qualification of this connection. The experimental program and the numerical models

were developed in the master's thesis of the first two authors [24]; this paper reprocesses those results, with the moment evaluated at the column face, and extends their interpretation.

The remainder of the paper is organized as follows. Section 2 describes the connection, Section 3 presents the FE model and the loading protocol, and Section 4 reports the experimental validation. Section 5 describes the parametric study, Section 6 discusses the results and Section 7 summarizes the conclusions.

2 Connection configuration

In a moment-resisting frame designed to resist seismic forces, structural redundancy requires frames with at least two bays, which leads to different connection conditions between beams and exterior or interior columns; the number of cases increases further in multistory buildings. This study addresses the connection between a floor beam and an exterior column, as shown in Fig. 1.

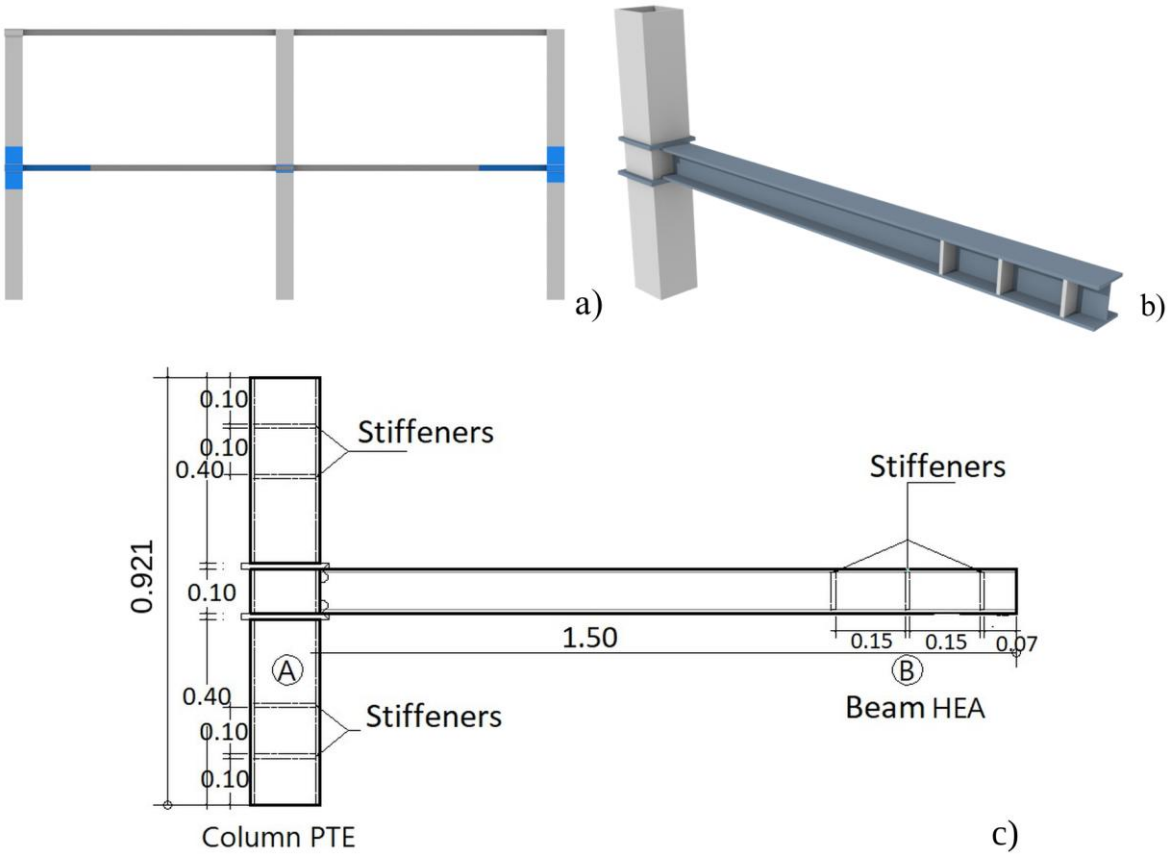
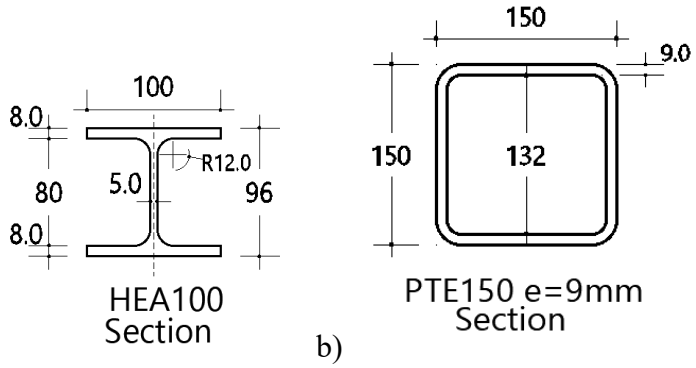


Fig. 1 Proposed connection: **a** location of the connection within the frame; **b** isometric view; **c** dimensions of the assembly (m)

The members correspond to sections available in the Colombian market and were selected according to the NSR-10 requirements for frames with moderate energy dissipation capacity

(DMO), which ensure compact sections. The beam is an HEA100 section of ASTM A572 Grade 50 steel, the column is a PTE150×150×9 section of ASTM A500 Grade C steel, and the continuity plates were cut from ASTM A572 Grade 50 steel plate. The column is continuous through the joint, and the plates are welded around its perimeter, so that they act as external diaphragms. The dimensions of the sections are shown in Fig. 2. Although the sections were selected for DMO frames, the connection was evaluated against the more demanding acceptance criteria for frames with special energy dissipation capacity (DES).



a) b)

Fig. 2 Cross sections (mm): **a** HEA100 beam; **b** PTE150×150×9 column

All joints were made with CJP arc welds using E70XX electrodes (F_{EXX} = 482 MPa). The welds were designed for the expected maximum strength of the connected elements, following AWS D1.1 [25], ANSI/AISC 341-16 [4], ANSI/AISC 360-16 [26] and NSR-10 [5].

3 Finite element model

The connection was analyzed with a three-dimensional FE model developed in ANSYS Mechanical APDL [27]. The cyclic loading protocol of NSR-10 (Section 3.5) was imposed as a sinusoidal displacement history using the transient solver. Since neither mass nor damping was defined, the analysis is equivalent to a quasi-static nonlinear analysis in which time acts only as a pseudo-time parameter. Material nonlinearity was included, whereas geometric nonlinearity (large displacements) was not considered.

3.1 Geometry

The model included a 1.5 m long beam and a 0.921 m tall column. The cross-sections were simplified by omitting the root and corner radii of the sections, and nominal thicknesses were used for the members and the continuity plates. The weld access holes were simplified as 20 mm square openings in the beam web (Fig. 3a). Three stiffeners spaced 150 mm apart were

modeled at the end of the beam, where the load is applied (Fig. 3b), and two internal stiffeners spaced 0.10 m apart were modeled inside the column near each support (Fig. 3c).

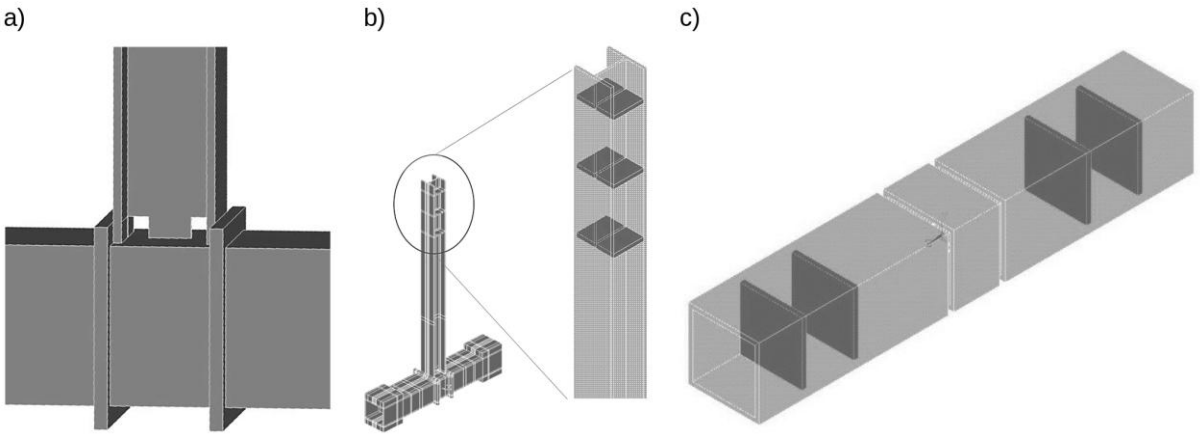


Fig. 3 Details of the FE model geometry: **a** weld access holes; **b** stiffeners at the load application point; **c** internal stiffeners of the column

The welds were modeled with a triangular cross-section at the following joints: column to continuity plates, both sides of the beam web to column, continuity plates to beam flanges, and beam flanges to column. Contact between the vertices of adjacent weld beads was avoided.

3.2 Element types and mesh

Two types of three-dimensional solid elements with three translational degrees of freedom per node were used. Eight-node hexahedral elements (SOLID185) were used in almost the entire volume, whereas SOLID186 elements in their ten-node tetrahedral form, with a node at each vertex and at the midpoint of each edge, were used in three bands that make the transition between zones meshed with different element sizes (Fig. 4).

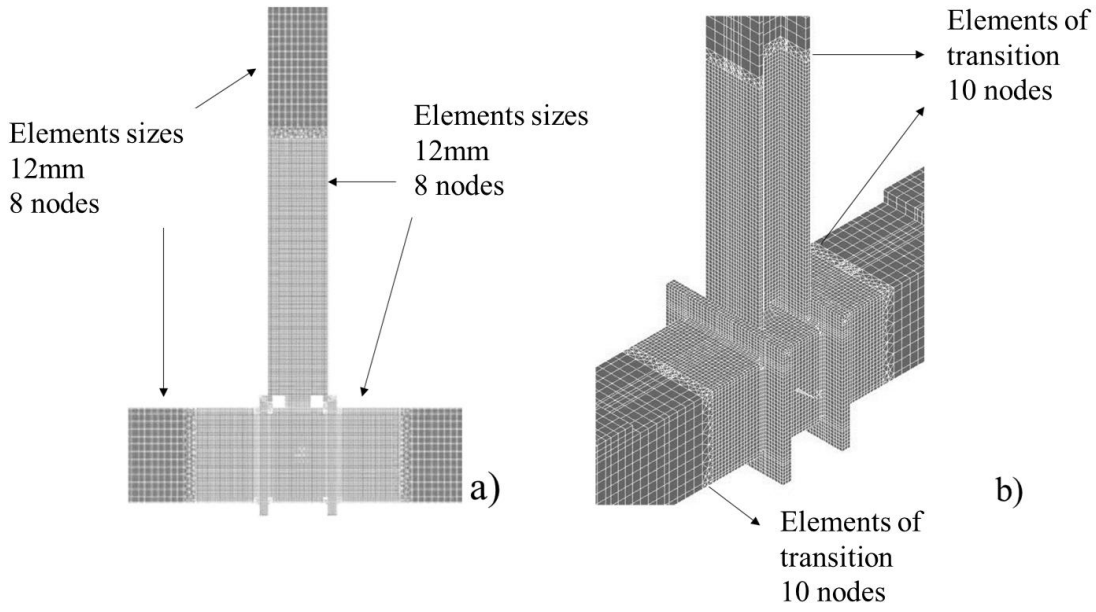


Fig. 4 FE mesh: **a** element sizes in the eight-node element zones; **b** transition bands with ten-node elements

The mesh was refined near the beam-to-column joint, where nonlinear material behavior was expected. The extent of the refined zone was defined with a preliminary model: it covered 500 mm of the beam and 150 mm of the column, measured from the boundary of the joint, which is approximately twice the extent of the plastified region. The maximum element size was 4 mm in the connection zone and 12 mm in the remaining volume. The mesh contained 90 844 eight-node elements and 8 198 ten-node elements. With a 4 mm element size, the plates of the connection zone are discretized with at least two elements through the thickness (beam flanges, 8 mm; column wall, 9 mm; continuity plates, 8–19 mm), and the beam web (5 mm) with one to two elements. The mesh quality check of ANSYS showed that only 0.03% of the elements exceeded the recommended aspect ratio limits. A formal mesh convergence study was not performed; the adequacy of the mesh is supported by the agreement with the full-scale test reported in Section 4.

3.3 Material models

Two constitutive models were defined for the steel. The first is a linear elastic material with a Young's modulus E = 200 000 MPa. The second represents the inelastic behavior through a multilinear stress–strain curve with four segments fitted to the average of the tensile test results (ASTM E8/E8M [28]) obtained for the steels of the validation specimen (Fig. 5), combined with an isotropic hardening rule (multilinear isotropic hardening). A Poisson's ratio of 0.3 was

adopted. The tensile tests were carried out on two specimens from the beam (flange and web), two from the column and one from the continuity plate.

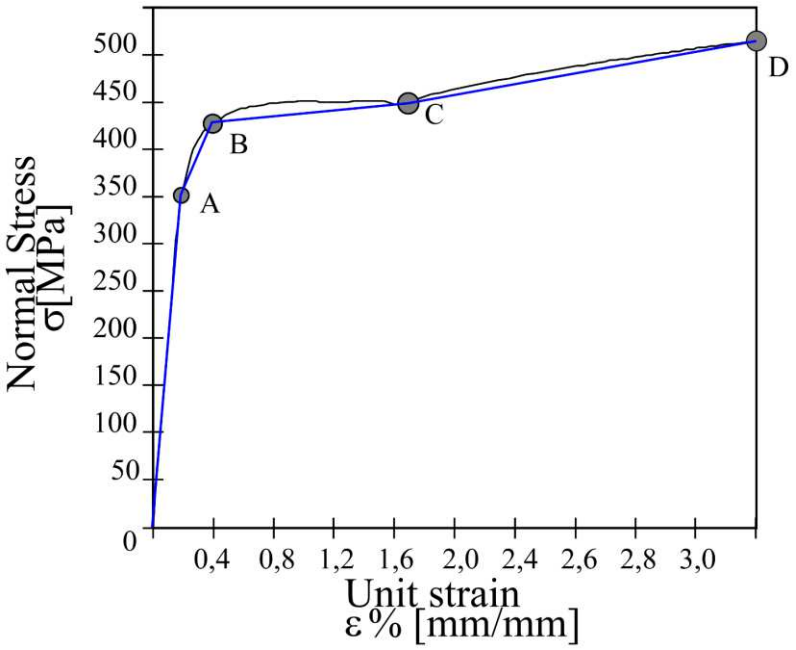


Fig. 5 Example of the definition of the multilinear model on the experimental stress–strain curve of one of the column specimens. A: proportional limit; B: yield point; C: end of the yield plateau; D: maximum stress

The nonlinear model was assigned to the beam, the column and the continuity plates within the connection zone, with the properties of each material listed in Table 1. A linear elastic model was assigned to the rest of the model, including the welds.

Table 1 Mechanical properties used in the FE model (measured values)

Element	E (MPa)	σ_A (MPa)	$\sigma_B = f_y$ (MPa)	σ_C (MPa)	σ_D (MPa)	ε_A	$\varepsilon_B = \varepsilon_y$	ε_C	ε_D
Beam	200 000	337.0	359.4	376.5	470.9	0.0017	0.0036	0.0280	0.0761
Column	200 000	359.0	441.9	460.0	580.1	0.0018	0.0041	0.0165	0.0622
Continuity plate	200 000	319.6	387.8	390.0	534.0	0.0016	0.0032	0.0170	0.0643

3.4 Boundary conditions and load application

The supports of the test were represented by 40 mm thick steel plates placed above and below each end of the column, with a stiffness ten times that of the column steel. Displacements perpendicular to the plane of the subassembly were restrained at both column ends to prevent torsion, and the displacement in the loading direction was restrained at one end (Fig. 6). In

addition, four linear elastic steel pads (150 mm wide, 3 mm thick and 300 mm high) were placed at the supports to represent the flexibility of the test supports, as explained in Section 4; these pads were kept in all the models of the parametric study. Because the connection rotation is computed from the relative displacements of the beam and the column (Eq. 1) and the subassembly is statically determinate, this support flexibility is not expected to affect the moment–rotation response of the connection significantly.

The imposed displacement was applied to a group of nodes coupled in the loading direction, located over a 9.5 mm wide strip at the load application point, to reproduce the hinged clevis of the actuator.

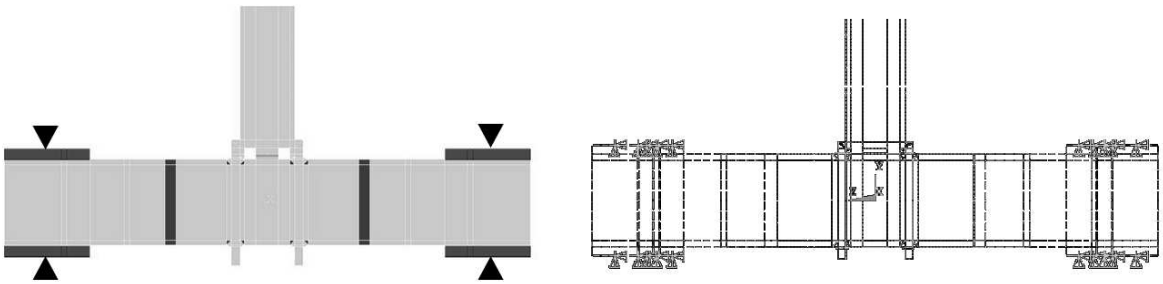


Fig. 6 Support plates and restraints of the FE model

3.5 Loading protocol

The cyclic loading protocol of NSR-10 for the qualification of beam-to-column moment connections, which follows ANSI/AISC 341 [4], was applied. The protocol is defined in terms of the drift angle θ, and the corresponding displacements at the load application point were computed from the distance between this point and the column axis, 1.341 m (Table 2).

Table 2 Loading protocol

Stage	Drift angle θ (rad)	Number of cycles	Displacement (mm)
1	0.00375	6	5.0
2	0.005	6	6.7
3	0.0075	6	10.1
4	0.010	4	13.4
5	0.015	2	20.1
6	0.020	2	26.8
7	0.030	2	40.2
8	0.040	2	53.7
9	0.050	2	67.1
10	0.060	2	80.5
11	0.070	2	94.0
12	0.080	2	107.5

4 Experimental validation

To validate the model, a full-scale connection with 190 mm square continuity plates 12.7 mm thick was tested under cyclic loading. The load was applied to the beam by an MTS dynamic actuator with a capacity of 100 kN, at 1.266 m from the column face (Fig. 7).

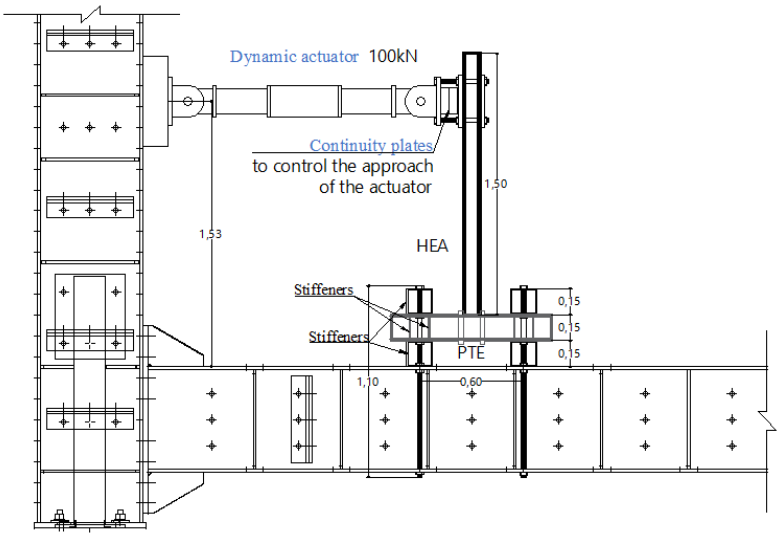


Fig. 7 Test setup for the full-scale connection test (dimensions in m)

The test was displacement-controlled and followed the loading protocol in Table 2, with a cycle period of 10 s (Fig. 8).

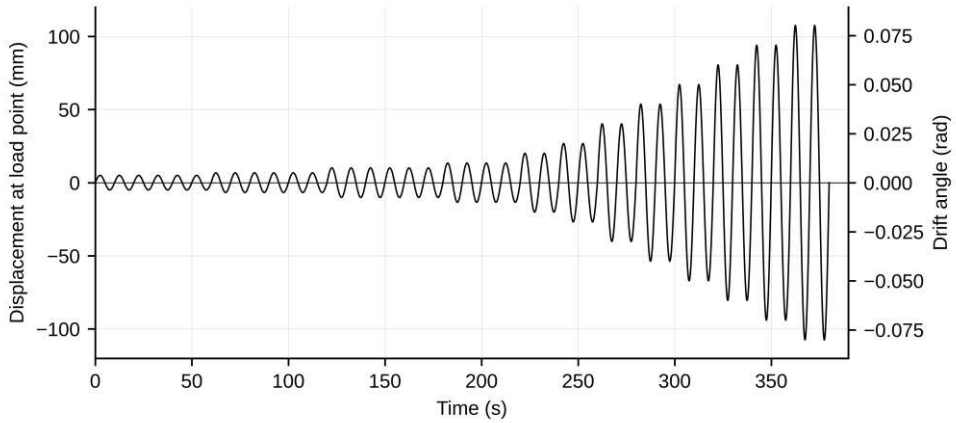


Fig. 8 Imposed displacement history (cycle period of 10 s)

Three linear variable differential transformers (LVDTs), located as shown in Fig. 9, were used to compute the connection rotation. LVDT 1 was placed on the beam at 243 mm from the column, and LVDTs 2 and 3 were placed on the column at 35.5 mm above the top of the beam and 35.5 mm below the bottom of the beam, respectively.

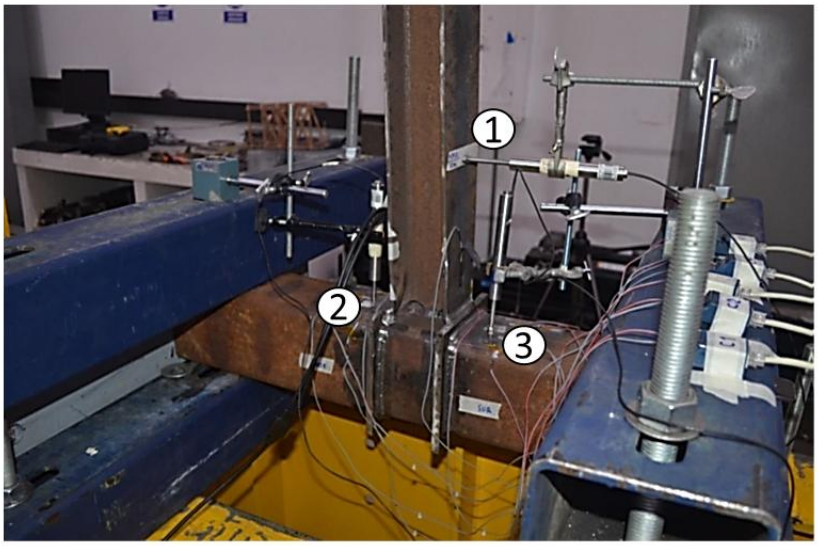


Fig. 9 Location of the LVDTs used as displacement control points

A first model with rigid supports reproduced the test well up to a load of about 30 kN, but overestimated the forces beyond that level. Video records of the test showed small slips and rotations at the supports. To represent this flexibility, the four linear elastic pads described in Section 3.4 were added at the supports; their dimensions were chosen so that the response of the model departed from that of the rigid-support model at about 30 kN. This calibration of the support flexibility is the only adjustment introduced in the model.

Fig. 10 compares the force–displacement curves of the test and of the calibrated model. The loading branches of the model agree closely with the test. The peak force of the model (37.8 kN) exceeds the experimental peak force by 2.6% in the positive direction (36.85 kN) and by 9.9% in the negative direction (−34.4 kN), where the test showed a lower capacity, probably due to the asymmetric behavior of the supports. The energy dissipated during the complete test was 43.4 kJ in the model and 40.7 kJ in the test (+6.7%). In terms of moment at the column face, the test reached 46.7 kN·m ($1.57M_p$, with M_p computed from the measured yield stress of the beam) and the model 47.8 kN·m ($1.61M_p$). The unloading stiffness of the model is higher than the experimental one, especially in the large-amplitude cycles, which is consistent with the isotropic hardening rule: it expands the yield surface and does not reproduce the Bauschinger effect, so that yielding upon load reversal is delayed. The specimen reached a drift angle of 0.08 rad without strength degradation; the peak force increased from 36.1 kN at 0.06 rad to 36.85 kN at 0.08 rad.

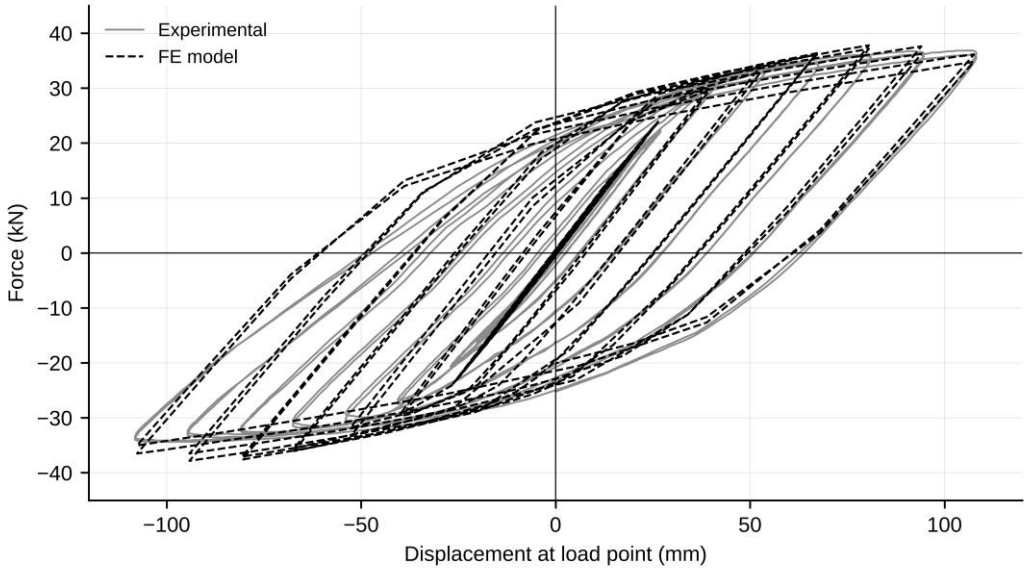


Fig. 10 Force–displacement response of the full-scale test and the calibrated numerical model

Fig. 11 shows the specimen before the test, with the two square continuity plates projecting beyond the faces of the column and the stiffeners at the load application point, and at the maximum imposed displacement. At that stage, the beam remained practically straight and its rotation concentrated at the end next to the continuity plates, which is consistent with the formation of a plastic hinge in the beam close to the connection. No local buckling of the beam flanges or continuity plates and no weld fracture were visible.

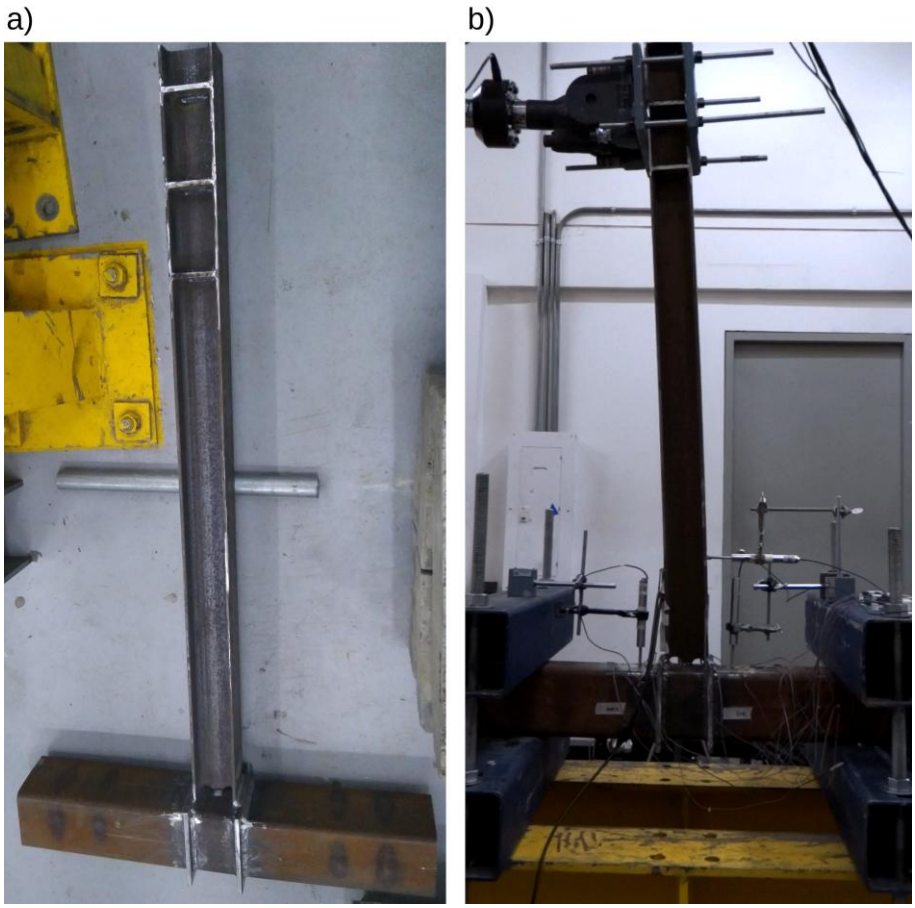


Fig. 11 Full-scale specimen: **a** before the test; **b** at the maximum imposed displacement (drift angle of 0.08 rad). Both photographs are oriented with the beam vertical, as in the test setup of Fig. 7

5 Parametric study of continuity plate size

5.1 Analyzed configurations

To assess the effect of the size of the continuity plates, 25 models were analyzed, combining five plate side lengths L and five plate thicknesses t_e (Table 3). Each configuration is designated L*xxx*E*yy*, where *xxx* is the side length and *yy* the thickness (*espesor*) in millimeters. Nominal material properties were used in these simulations.

Table 3 Designation of the analyzed continuity plate configurations

Side length L (mm)	Thickness t_e (mm)				
	8	9	12.7	15	19
180	L180E8	L180E9	L180E12.7	L180E15	L180E19
190	L190E8	L190E9	L190E12.7	L190E15	L190E19
200	L200E8	L200E9	L200E12.7	L200E15	L200E19
210	L210E8	L210E9	L210E12.7	L210E15	L210E19
220	L220E8	L220E9	L220E12.7	L220E15	L220E19

5.2 Moment–rotation response

For each configuration, the moment M was plotted against the relative rotation θ between the beam and the column. The rotation was computed with Eq. (1) from the displacements at the control points shown in Fig. 9:

$$\theta = \tan^{-1}\left(\frac{\Delta_1}{L_1}\right) - \tan^{-1}\left(\frac{\Delta_2 - \Delta_3}{L_{23}}\right) \quad (1)$$

where Δ_1 is the beam displacement, Δ_2 and Δ_3 are the column displacements, L_1 is the distance from the column axis to the control point of Δ_1, and L_{23} is the distance between the control points of Δ_2 and Δ_3. The moment at the column face was computed with Eq. (2) from the reaction force F obtained in the model and the distance L_f = 1.266 m between the load application point and the column face, which is the section at which NSR-10 [5] and ANSI/AISC 341 [4] evaluate the flexural resistance of the connection:

$$M = F \cdot L_f \quad (2)$$

As an example, Fig. 12 shows the hysteresis loops of the moment–rotation curve of configuration L180E8, together with the yield moment M_y, the plastic moment M_p of the beam and the $0.8M_p$ limit.

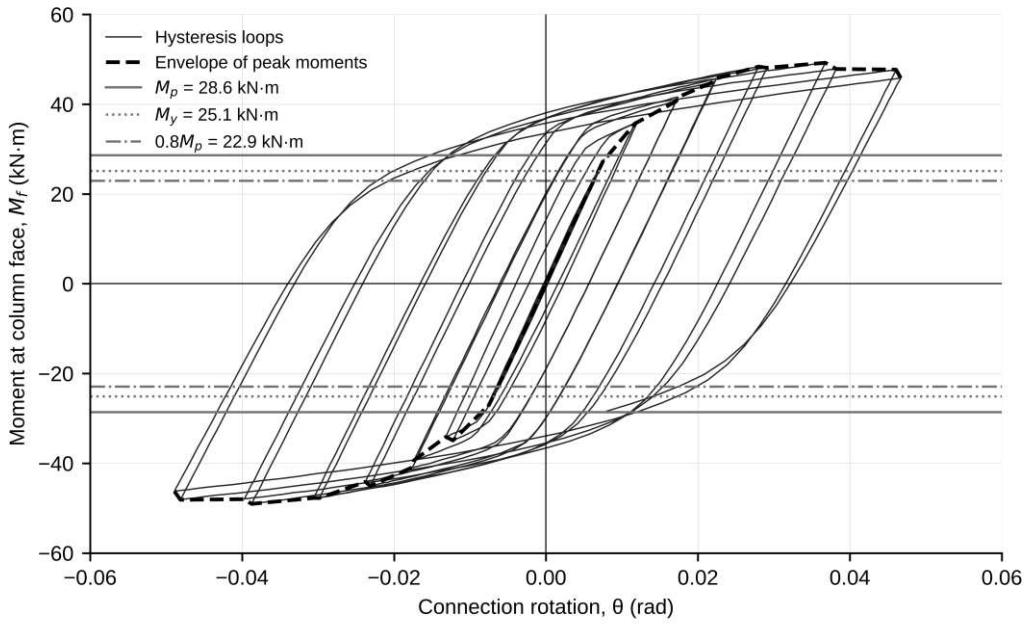


Fig. 12 Moment at the column face versus connection rotation for configuration L180E8 (nominal material properties)

6 Results and discussion

6.1 Flexural resistance at the column face

Table 4 lists the maximum moment at the column face, $M_{f,max}$, reached during the hysteresis cycles of each configuration. Because these models use nominal material properties, the moments are compared with the nominal plastic moment of the beam, $M_p = Z_x F_y = 83\ cm^3 \times 345\ MPa = 28.64\ kN{\cdot}m$. The maximum moment increases with the side length of the continuity plates, from 49.0–49.2 kN·m for L = 180 mm to 50.6–50.7 kN·m for L = 220 mm ($1.71M_p$ to $1.77M_p$), whereas the effect of the thickness is negligible (at most 0.3 kN·m for a given side length). The increase is largest between 180 and 190 mm and decreases progressively for larger plates, which indicates that the plate size is most influential when it is close to the width of the column (150 mm). The overstrength of about 1.7 is consistent with the experimental result ($1.57M_p$ with the measured yield stress) and reflects the strain hardening of the beam steel up to its tensile strength.

NSR-10 [5] and ANSI/AISC 341 [4] require that, for frames with special energy dissipation capacity, the flexural resistance measured at the column face be at least $0.8M_p$ at a story drift angle of 0.04 rad. Table 5 shows the moment at the column face when the connection rotation of Eq. (1) reached 0.04 rad, which ranged from $1.64M_p$ to $1.71M_p$, that is, more than twice the required value in all configurations. Since the connection rotation is only part of the story drift, this rotation is reached at a drift larger than 0.04 rad; because the moment decreases only slightly after its peak (Fig. 12), the check is conservative.

Table 4 Maximum moment at the column face, $M_{f,max}$ (kN·m)

Side length L (mm)	Thickness t_e (mm)				
	8	9	12.7	15	19
180	49.2	49.2	49.1	49.1	49.0
190	49.9	49.9	49.9	49.9	49.9
200	50.1	50.2	50.2	50.3	50.3
210	50.4	50.4	50.4	50.5	50.5
220	50.6	50.7	50.7	50.7	50.7

Table 5 Moment at the column face at a connection rotation of 0.04 rad, normalized by the nominal plastic moment of the beam (M_p = 28.64 kN·m). Required minimum for DES frames: 0.8

Side length L (mm)	Thickness t_e (mm)				
	8	9	12.7	15	19
180	1.66	1.67	1.65	1.64	1.64
190	1.69	1.69	–[a]	1.69	1.68

Side length L (mm)	Thickness t_e (mm)				
	8	9	12.7	15	19
200	1.70	1.70	1.69	1.69	1.69
210	1.70	1.70	1.70	1.70	1.70
220	1.71	1.71	1.70	1.70	1.69

[a] Not reported: the detailed output available for this configuration is inconsistent with its summary results.

6.2 Initial rotational stiffness

The initial rotational stiffness K_i was computed as the secant stiffness M_f/θ at the peak of the first cycles of the protocol (drift angle of 0.00375 rad), where the moment at the column face (5.4–5.7 kN·m) is well below the yield moment and the response is elastic. Table 6 lists the values for the configurations with t_e = 19 mm and different side lengths, and for those with L = 220 mm and different thicknesses. The stiffness increases with both parameters: increasing the side length from 180 to 220 mm raises K_i by 13%, and increasing the thickness from 8 to 19 mm raises it by 17%. Therefore, unlike the maximum moment, the initial stiffness is sensitive to the plate thickness.

Table 6 Initial rotational stiffness K_i (kN·m/rad), computed with the moment at the column face

Fixed parameter	Varied parameter (mm)	K_i (kN·m/rad)
t_e = 19 mm	180	4184
	190	4359
	200	4439
	210	4577
	220	4741
L = 220 mm	8	4039
	9	4113
	12.7	4439
	15	4544
	19	4741

6.3 Dissipated energy

For each configuration, the energy dissipated by the connection was computed with Eq. (3) as the area enclosed by the hysteresis loops of the curve of moment at the column face versus rotation, limited to rotations between −0.04 and +0.04 rad:

$$E = \int_0^{0.04\ \mathrm{rad}} M\ \mathrm{d}\theta \tag{3}$$

The results are presented in Table 7 and Fig. 13. The dissipated energy increases with the plate thickness and decreases with the plate side length. For a given side length, increasing the thickness from 8 to 19 mm raises the dissipated energy by 3.6–4.9%, whereas for a given thickness, increasing the side length from 180 to 220 mm reduces it by 10.0–11.2%. Among the assessed configurations, the largest dissipated energy (5.19 kJ) corresponds to the shortest and thickest plates (L180E19), and the smallest (4.45 kJ) to the longest and thinnest plates (L220E8). A plausible explanation is that longer plates stiffen the joint region and reduce the inelastic deformation developed for a given rotation, which should be confirmed by examining the distribution of plastic strains. These trends reveal a trade-off for design: longer plates increase the maximum moment but reduce the energy dissipated within ±0.04 rad, whereas thicker plates increase energy dissipation with little effect on strength.

Table 7 Energy dissipated within ±0.04 rad, computed with the moment at the column face (kJ)

Side length L (mm)	Thickness t_e (mm)				
	8	9	12.7	15	19
180	5.01	5.03	5.09	5.14	5.19
190	4.82	4.86	4.97	5.00	5.07
200	4.69	4.72	4.81	4.86	4.91
210	4.55	4.58	4.68	4.71	4.77
220	4.45	4.49	4.58	4.61	4.67

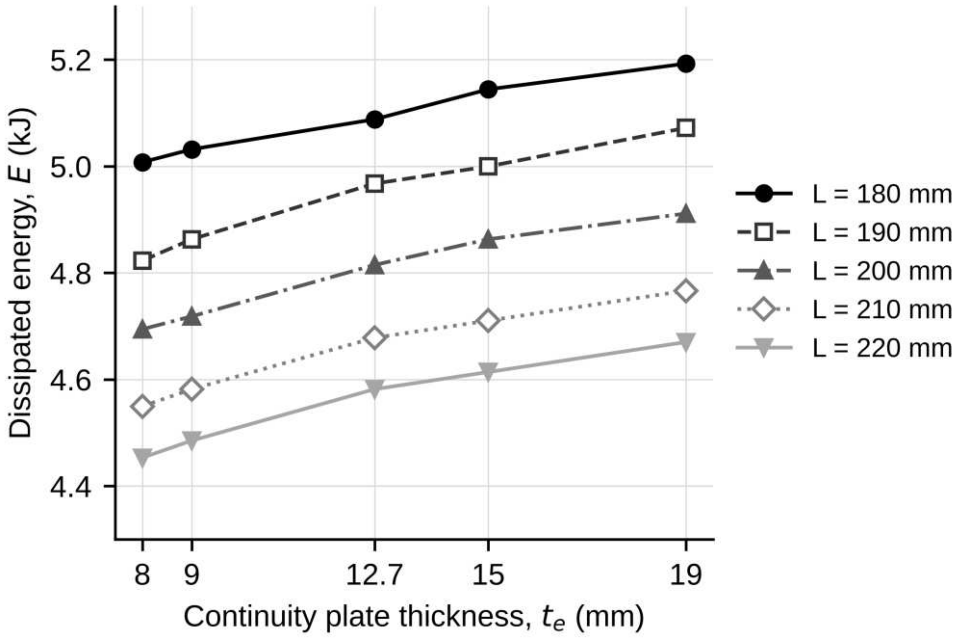


Fig. 13 Energy dissipated within ±0.04 rad as a function of the continuity plate thickness for each side length

7 Conclusions

A welded moment connection between an HEA100 beam and a PTE150×150×9 square HSS column with two square continuity plates was studied with a nonlinear FE model validated against a full-scale cyclic test. Twenty-five combinations of plate side length and thickness were analyzed. The main conclusions are as follows:

- After calibrating the flexibility of the test supports, the FE model reproduced the experimental force–displacement response with differences of 2.6% in the positive peak force and 6.7% in the dissipated energy, although it overestimated the unloading stiffness in the large-amplitude cycles.
- All 25 configurations, analyzed with nominal material properties, satisfied the requirement of NSR-10 for frames with special energy dissipation capacity (DES): the moment at the column face at a connection rotation of 0.04 rad was $1.64M_p$ to $1.71M_p$, compared with the required $0.8M_p$, even though the sections were selected according to the compactness requirements for moderate energy dissipation capacity (DMO).
- The maximum moment at the column face depends mainly on the side length of the continuity plates and is practically insensitive to their thickness: it increased from $1.71M_p$ to $1.77M_p$ as the side length increased from 180 to 220 mm, with the largest variation when the plate size was close to the column width.
- The initial rotational stiffness increases with both the side length and the thickness of the plates: by 13% when the side length increased from 180 to 220 mm and by 17% when the thickness increased from 8 to 19 mm.
- The energy dissipated within ±0.04 rad, computed as the area enclosed by the moment–rotation hysteresis loops, increases with the plate thickness and decreases with the plate side length, varying between 4.45 and 5.19 kJ.

These results provide a basis for the future qualification of this connection, subject to the following limitations. The conclusions apply to the analyzed sections and to an exterior connection without column axial load. The numerical model was validated against a single specimen, and the flexibility of the test supports was represented by calibrated elastic pads. Geometric nonlinearity was not included, so local buckling could not be captured; this simplification is supported by the compactness of the beam (flange width-to-thickness ratio $b/2t_f = 6.25$, below the limit of 7.35 for highly ductile members of ANSI/AISC 341-16 [4]) and by the absence of strength degradation in the test up to 0.08 rad, but it may not hold for other sections. No formal mesh convergence study was carried out, and the isotropic hardening rule

overestimates the unloading stiffness. Further cyclic tests with different plate sizes, models with combined isotropic–kinematic hardening, geometric nonlinearity and fracture of welds and base metal, and the assessment of interior connections are recommended.

Statements and Declarations

Funding The authors did not receive support from any organization for the submitted work.

Competing interests The authors have no relevant financial or non-financial interests to disclose.

Author contributions William G. Piraquive and Miguel A. Morales - performing experimental and numerical study, writing the original draft, formal analysis, funding acquisition. Fabián Lamus - conceptualization, methodology, supervision, writing original draft, review and editing. Federico A. Nuñez - Methodology, formal analysis, review and editing.

Data availability The data that support the findings of this study are available from the corresponding author upon reasonable request.

Ethics approval Not applicable.

Acknowledgements The authors thank Eng. Jenny M. Pira for her assistance in preparing the figures of this paper. They also thank the Structures Laboratory of the Department of Civil Engineering of the Pontificia Universidad Javeriana, where the full-scale connection test and the flexural tests of the members were performed, and the Laboratory of Mechanical Testing and Plastic Deformation of the Faculty of Engineering of the Universidad Nacional de Colombia, Bogotá, where the tensile tests were carried out, for their technical support.

References

1. Mahin SA (1998) Lessons from damage to steel buildings during the Northridge earthquake. Eng Struct 20(4–6):261–270. https://doi.org/10.1016/S0141-0296(97)00032-1
2. Federal Emergency Management Agency (2000) Recommended seismic design criteria for new steel moment-frame buildings, FEMA-350. Federal Emergency Management Agency, Washington, DC
3. American Institute of Steel Construction (2016) Prequalified connections for special and intermediate steel moment frames for seismic applications, ANSI/AISC 358-16. American Institute of Steel Construction, Chicago, IL
4. American Institute of Steel Construction (2016) Seismic provisions for structural steel buildings, ANSI/AISC 341-16. American Institute of Steel Construction, Chicago, IL
5. Asociación Colombiana de Ingeniería Sísmica (2010) Reglamento Colombiano de Construcción Sismo Resistente NSR-10. Ministerio de Ambiente, Vivienda y Desarrollo Territorial, Bogotá

6. Fadden MF (2013) Cyclic bending behavior of hollow structural sections and their application in seismic moment frame systems. Dissertation, University of Michigan
7. Fadden M, McCormick J (2012) Cyclic quasi-static testing of hollow structural section beam members. J Struct Eng 138(5):561–570. https://doi.org/10.1061/(ASCE)ST.1943-541X.0000506
8. D'Aniello M, Güneyisi EM, Landolfo R, Mermerdaş K (2014) Analytical prediction of available rotation capacity of cold-formed rectangular and square hollow section beams. Thin-Walled Struct 77:141–152. https://doi.org/10.1016/j.tws.2013.09.015
9. Packer JA, Wardenier J, Zhao XL, van der Vegte GJ, Kurobane Y (2009) Design guide for rectangular hollow section (RHS) joints under predominantly static loading, 2nd edn. CIDECT Design Guide 3. Comité International pour le Développement et l'Étude de la Construction Tubulaire, Geneva
10. Kurobane Y, Packer JA, Wardenier J, Yeomans N (2004) Design guide for structural hollow section column connections. CIDECT Design Guide 9. TÜV-Verlag, Cologne
11. Ting LC, Shanmugam NE, Lee SL (1991) Box-column to I-beam connections with external stiffeners. J Constr Steel Res 18(3):209–226. https://doi.org/10.1016/0143-974X(91)90026-W
12. Shanmugam NE, Ting LC, Lee SL (1991) Behaviour of I-beam to box-column connections stiffened externally and subjected to fluctuating loads. J Constr Steel Res 20(2):129–148. https://doi.org/10.1016/0143-974X(91)90016-T
13. Qin Y, Chen Z, Yang Q, Shang K (2014) Experimental seismic behavior of through-diaphragm connections to concrete-filled rectangular steel tubular columns. J Constr Steel Res 93:32–43. https://doi.org/10.1016/j.jcsr.2013.10.020
14. Bagheri Sabbagh A, Chan TM, Mottram JT (2013) Detailing of I-beam-to-CHS column joints with external diaphragm plates for seismic actions. J Constr Steel Res 88:21–33. https://doi.org/10.1016/j.jcsr.2013.05.006
15. Ramirez Ortiz C, Areiza Palma G, Gutierrez Amador AD, Ramirez Duque JL, Cano Buitron RE, Gonzales Escobar LF (2022) Seismic behavior of a steel beam-to-concrete-filled steel tubular column connection using external diaphragms. Appl Sci 12(7):3618. https://doi.org/10.3390/app12073618
16. Ramírez Ortiz C, Gutierrez Amador AD, Ramírez Duque JL (2022) Numerical analysis of the seismic behavior of a steel beam-to-concrete-filled steel tubular column connection using external diaphragms. Buildings 12(8):1217. https://doi.org/10.3390/buildings12081217
17. Díaz C, Victoria M, Martí P, Querin OM (2011) FE model of beam-to-column extended end-plate joints. J Constr Steel Res 67(10):1578–1590. https://doi.org/10.1016/j.jcsr.2011.04.002
18. Del Savio AA, Nethercot DA, Vellasco PCGS, Andrade SAL, Martha LF (2009) Generalised component-based model for beam-to-column connections including axial versus moment interaction. J Constr Steel Res 65(8–9):1876–1895. https://doi.org/10.1016/j.jcsr.2009.02.011
19. López-Colina C, Serrano MA, Lozano M, López Gayarre F, Suárez JM, Wilkinson T (2019) Characterization of the main component of equal width welded I-beam-to-RHS-column connections. Steel Compos Struct 32(3):337–346. https://doi.org/10.12989/scs.2019.32.3.337
20. Di Benedetto S, Latour M, Francavilla AB, Rizzano G (2023) Cyclic behaviour of 3D cut welded connections with CHS columns and through I-beams. ce/papers 6(3–4):1464–1469. https://doi.org/10.1002/cepa.2263
21. Latour M, Sato A, Ajwad A, Di Benedetto S, Rizzano G (2025) Cyclic response of moment resisting joints for tubular structures with passing-through beams. In: Proceedings of the International Colloquium on Stability and Ductility of Steel Structures (SDSS 2025), Barcelona

22. Tjahjanto H, MacRae G, Abu A, Clifton C, Beetham T, Mago N (2019) Diaphragm axial capacity for external diaphragm connections (EDCs) in square CFST column structures. Bull N Z Soc Earthq Eng 52(3):134–140. https://doi.org/10.5459/bnzsee.52.3.134-140
23. Andrade C (2015) Calificación de conexiones de perfiles I de acero: viga conectada al eje débil. Master's thesis, Universidad Nacional de Colombia
24. González Piraquive W, Morales Lascano MA (2018) Determinación numérica de la influencia del tamaño de las placas de continuidad en la respuesta histerética de una conexión viga HEA – columna PTE para PRM. Master's thesis, Pontificia Universidad Javeriana
25. American Welding Society (2015) Structural welding code—steel, AWS D1.1/D1.1M:2015. American Welding Society, Miami, FL
26. American Institute of Steel Construction (2016) Specification for structural steel buildings, ANSI/AISC 360-16. American Institute of Steel Construction, Chicago, IL
27. ANSYS Inc. (2015) ANSYS Mechanical APDL, Release 16.2. ANSYS Inc., Canonsburg, PA
28. ASTM International (2016) Standard test methods for tension testing of metallic materials, ASTM E8/E8M-16a. ASTM International, West Conshohocken, PA